
OCTOBER
14-17
MWP 2025
International Topical Meeting
on Microwave Photonics
Centre des Congrès de Québec, Canada
mwp2025.org
Program

# TABLE OF CONTENT - TABLE DES MATIÈRES




**MWP 2025 - Secretariat**: mwp2025@conferium.com

| Tuesday, October 14, 2025 - Mardi le 14 octobre 2025 | | Room / Salle |
|---|---|---|
| 12:00 - 18:45 | Registration - Inscription Welcome Desk | Urban Space |
| 13:00 - 15:00 | Workshop 1 - New frontiers in neuromorphic photonics | 309AB |
| 15:00 - 15:30 | Coffee Break - Pause-café | Urban Space |
| 15:30 - 18:30 | Workshop 2 - Photonic control of antennas | 309AB |

| Wednesday, October 15, 2025 - Mercredi le 15 octobre 2025 | | Room / Salle |
|---|---|---|
| 07:00 - 20:00 | Registration - Inscription Welcome Desk | Urban Space |
| 08:15 - 10:00 | Welcome and Plenary Session 1 | 309AB |
| 10:00 - 10:30 | Coffee Break - Pause-café | Urban Space |
| 10:30 - 12:15 | We1 - Photonic microwave processing, sensing, and measurements 1 | 309AB |
| 12:15 - 13:30 | Lunch (included) - Repas du midi (inclus) | Urban Space |
| 13:30 - 15:15 | We2 - High-speed photomixers and optoelectronic converters and Tutorial | 309AB |
| 15:15 - 16:45 | Coffee Break and We3 - Poster Session 1 | Urban Space |
| 16:45 - 18:25 | We4 - High-performance microwave photonic signal sources 1 | 309AB |
| 18:30 - 20:30 | Welcome Reception - Réception de bienvenue | Urban Space |

| Thursday, October 16, 2025 - Jeudi le 16 octobre 2025 | | Room / Salle |
|---|---|---|
| 08:00 - 18:30 | Registration - Inscription Welcome Desk | Urban Space |
| 08:30 - 10:00 | Plenary Session 2 and Invited | 309AB |
| 10:00 - 10:30 | Coffee Break - Pause-café | Urban Space |
| 10:30 - 12:15 | Th1 - Photonic-enhanced artificial intelligence (AI) computing techniques | 309AB |
| 12:15 - 13:30 | Lunch (included) - Repas du midi (inclus) | Urban Space |
| 13:30 - 15:00 | Th2 - Integrated microwave photonics | 309AB |
| 15:15 - 16:45 | Coffee Break and Th3 - Poster Session 2 | Urban Space |
| 16:45 - 18:15 | Th4 - Radio over Fiber (RoF) for B5G/6G mobile data and terrestrial communication systems | 309AB |
| 18:30 - 21:30 | Award Banquet Evening - Banquet de remise de prix | Monastère des Augustines |

| Friday, October 17, 2025 - Vendredi le 17 octobre 2025 | | Room / Salle |
|---|---|---|
| 08:00 - 16:30 | Registration - Inscription Welcome Desk | Urban Space |
| 08:30 - 10:00 | Plenary Session 3 and Invited | 309AB |
| 10:00 - 10:30 | Coffee Break - Pause-café | Urban Space |
| 10:30 - 12:15 | Fr1 - High-performance microwave photonic signal sources 2 | 309AB |
| 12:15 - 13:30 | Lunch (included) - Repas du midi (inclus) | Urban Space |
| 13:30 - 15:00 | Fr2 - Photonic microwave processing, sensing, and measurements 2 | 309AB |
| 15:00 - 15:30 | Coffee Break - Pause-café | Urban Space |
| 15:30 - 16:15 | Fr3 - Postdeadline Session and Wrap-Up | 309AB |

11:30 - 11:45 **AI-COMPUTING THROUGH LOW-CONSUMPTION VCSEL-BASED ANALOG RADIO-OVER-FIBER SYSTEM**
**Jacopo Nanni**, Department of Electrical, Electronic and Information Engineering (DEI), University of Bologna, Italy
Jacopo Nanni, Siqi Wang, Aziz Benlarbi Delai, Giovanni Tartarini

11:45 - 12:00 **DEMONSTRATION OF DUAL-PUMP DEGENERATE OPTICAL PARAMETRIC OSCILLATION IN KERR MICRORESONATORS FOR INTEGRATED COHERENT ISING MACHINES**
**Kambiz Jamshidi**, TU Dresden, Germany
Menglong He, Mohd Saif Shaikh, Abdou Shetewy, Kambiz Jamshidi

12:00 - 12:15 **IMAGE CLASSIFICATION WITH A SIMPLE PHOTONIC PERCEPTRON BASED ON HETERODYNE DETECTION**
**Miguel Cuenca Piqueras**, Engineering Research Institute I3E Univ. Miguel Hernández, Spain
Miguel Cuenca Piqueras, Carlos Fernandez-Pousa, Hugues Guillet de Chatellus

## TH2 - INTEGRATED MICROWAVE PHOTONICS

**Co-chairs: Xinyi Zhu**

**Hao Sun**

13:30 - 14:00 **INTEGRATED NONLINEAR LITHIUM NIOBATE PHOTONIC CIRCUITS: TOWARDS ULTRAFAST, LOW-POWER, AND SCALABLE LIGHT'MATTER INTERFACES**
**Ian Christen**, University of California, Berkeley, United States of America
Mengjie Yu, Ian Christen
**Invited Speaker**

14:00 - 14:15 **DEMONSTRATION OF AN INP-SOI HETEROGENEOUSLY INTEGRATED DISTRIBUTED COHERENT RADAR SYSTEM**
**Luca Rinaldi**, CNIT, Italy
Valentina Gemmato, Federico Camponeschi, Filippo Scotti, Luca Rinaldi, Muhammad Imran, Claudio Porzi, Paolo Ghelfi, Mirco Scaffardi, Antonella Bogoni

14:15 - 14:30 **A SILICON PHOTONIC CHIP FOR SIMULTANEOUS MICROWAVE AND NEAR-INFRARED DUAL-BAND BEAMFORMING**
**Ruiqi Zheng**, Jinan University, China (People's Republic of)
Ruiqi Zheng, Jingxu Chen, Jinkun Hu, Haikun Huang, Jiejun Zhang, Jianping Yao

14:30 - 14:45 **FINE-GRAINED DIFFRACTIVE SLAB FOR ACCURATE AND LOW-COMPLEXITY ON-CHIP PHOTONIC CONVOLUTION**
**Shen Zichao**, Chinese Academy of Sciences, China (People's Republic of)
Shen Zichao, Weichao Ma, Ruixuan Wang, Wangzhe Li

# Image classification with a simple photonic perceptron based on heterodyne detection

Miguel Cuenca Piqueras
*Engineering Research Institute I3E*
*Univ. Miguel Hernández*
03202 Elche, Spain
miguel.cuenca02@goumh.umh.es

Carlos R. Fernandez-Pousa
*Engineering Research Institute I3E*
*Univ. Miguel Hernández*
03202 Elche, Spain
c.pousa@umh.es

Hugues Guillet de Chatellus
*Institut FOTON*
*Univ. Rennes, CNRS*
35402 Rennes, France
hugues.guilletdechatellus@univ-rennes.fr

***Abstract*— The use of photonic architectures to build neural networks is a fast-growing field, both because these systems offer huge computing potential, and because the power consumption of photonic systems is much lower than that of their electronic equivalents. In this context, we have developed a simple architecture based on a simple heterodyne interferometer, enabling vector multiplication. This architecture enables us to process images in the time domain, and perform image classification tasks. More importantly, the building block we propose can be generalized to multi-heterodyne architectures, enabling ultra-high rate matrix computation for neural network layers, and accelerators for convolutional neural networks.**

***Keywords—perceptron, neural network, heterodyne detection, analog computing, matrix calculation***

## I. Introduction

Artificial neural networks are at the heart of artificial intelligence systems. They have enabled a spectacular revival of analog computing, enabling classification, recognition, and prediction tasks. Paradoxically, these architectures are commonly implemented in digital electronics, which raises important concerns about power consumption and ultimate performance. On the contrary, photonic systems can process radio or microwave signals in an analog manner, with remarkable energy efficiency and very large bandwidth. In this context, it is obvious that optics is capable of providing effective hardware solutions for artificial intelligence, and indeed a large number of neuromorphic photonic systems have been presented over the past ten years [1].

The basic building block of these architectures is the perceptron, or artificial neuron, whose function is to combine a number of inputs, weight them by coefficients, and produce an output via an (generally non-linear) activation function (Fig. 1, top). Training the perceptron consists of determining the weight coefficients according to the intended objective. In the case of image classification, the system is trained on a large database (images), so that it can then classify any unknown image. In most of analog implementations of the perceptron, the training stage is implemented offline, and the perceptron simply calculates the product of the input data with the weighting coefficients. Several photonic implementations of perceptrons have been reported so far, including space-optics based approaches [2-4].

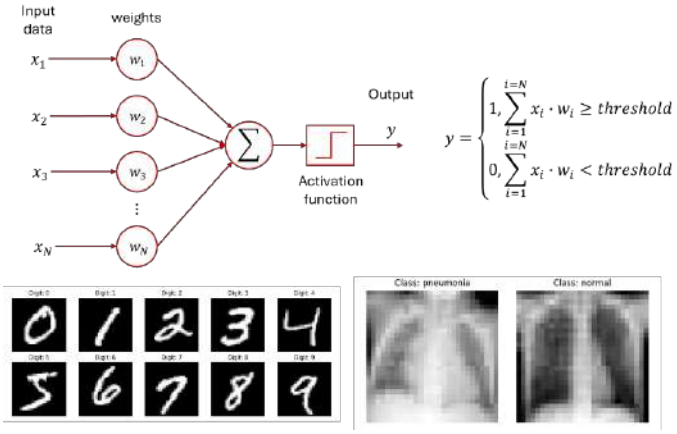


Fig. 1. Top: generic perceptron architecture. The input data ($x_i$) is multiplied with the synaptic weights ($w_i$) optimized off-line for the specific application. The neuron computes the weighted sum ($\Sigma_i\, x_i w_i$). An activation function generates the output ($y$) of the perceptron. Bottom: samples of the 0-9 digit classes and of the binary classes pneumonia / normal used in the image classification experiments.

Here, we propose a new and simple implementation of a photonic perceptron operating in the time domain and dedicated to image classification. Two proof-of-concept implementations are presented, oriented to digit classification and pneumonia detection in gray-scale images (Fig. 1, bottom). Our architecture is based on heterodyne detection and standard microwave photonics concepts, and as such offers multiple prospects for future neuromorphic photonic processing, including the processing of complex data, potential for parallelization, and the reach of ultra-high computation speeds based in on-chip architectures.

## II. Architecture

The architecures essentially consists in a simple heterodyne fiber interferometer. A CW laser (1550 nm) is split in two arms. Electro-optic amplitude modulators (i.e. Mach-Zehnder interferometers biaised at null) are inserted in the two arms, while an optical frequency shifter is inserted in one of them (Fig. 2, top). Both arms are recombined of a balanced photodetector (1.6 GHz bandwidth). The resulting signal is then sampled and processed digitally. Both the input matrix data and the synaptic weights are serialized in the time domain, and applied to the

 

modulators by means of an arbitrary waveform synthesizer. The samping rate of the input waveforms is 125 MSa/s for the MNIST dataset and 100 MSa/s for the PneumoniaMNIST dataset. These rates are chosen to match the bandwidth limitations of the AWG and to ensure synchronization with the acquisition system. In particular, the digitizer sampling rates (0.2 - 0.25 GSa/s) are selected as integer multiples of the waveform sampling rates to guarantee alignment across the traces. The frequency shifter is driven at $f_s = 80$ MHz.

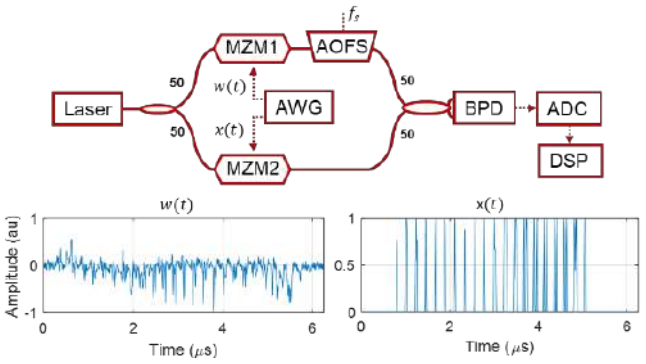


Fig. 2. Top: sketch of the photonic perceptron. A CW laser is split in two. Each arm contains an amplitude modulator (MZM1 and MZM2). The first arm also incorportes a frequency shifter (AOFS). Both arms are recombined of a balanced photodiode (BPD). The detection signal is digitized (ADC) and processed numerically (DSP). Bottom: examples of the (bipolar) weight vector $w(t)$ and the (unipolar) input data $x(t)$ serialized in time.

The weight functions used to encode the synaptic connections are obtained by training simple perceptrons in software. The original image data are first serialized into one-dimensional input vectors. Both weight and image data are predeced by an overhead of reference symbols, as explained below. Each perceptron is trained using the appropriate activation function based on the task. For digit classification (i.e. identification of the digit '6' among digits '0' through '9', using the MNIST dataset [5]), a linear activation function is used to train the system. The training is performed on the full training subset, with each 28×28 pixel image flattened into a 784-element input vector. The model is then evaluated on 1,000 images from the MNIST test set. These same images are used in the photonic experimental setup, enabling direct comparison between computational and physical implementations of the classification procedure. For pneumonia detection, the PneumoniaMNIST dataset is used, consisting of 64×64 grayscale medical images [6]. A sigmoid activation function is employed for perceptron training. A subset of 460 test images is selected and evaluated in both the software and photonic domains using the same procedure. In both experiments, confusion matrices are computed to evaluate classification performance and to quantify the agreement between digital simulations and experimental photonic outputs.

## III. Signal Processing and Image Classification

According to Fig. 2, the output of the BPD is:

$$I_{BPD}(t) = I_0 \cos(2\pi f_s t + \varphi) \sum_{k=-\infty}^{+\infty} s_k(t - kT) \qquad (1)$$

with $I_0$ the optical input power, $f_s$ the frequency shift, and $\varphi = \omega_0 \tau_{interf} + \theta - \pi/2$ the phase shift, where $\omega_0$ is the optical carrier frequency, $\tau_{interf}$ the interferometer's time imbalance, and $\theta$ the RF phase of the tone driving the AOFS. In this expression, the RF tone at $f_s$ modulates a stream of symbols $s_k$ of duration $T$ signaled with square (NRZ) pulses. This stream is organized in groups of $M$ symbols $s_k$ representing the product of image data $x_k$ and weights $w_k$, $s_k = x_k \times w_k$. In the MZMs, the images are preceded by an overhead of nine reference images of the form [0, 0, 0, +1, 0, +1, 0, 0, 0], each of length $M$, and nine reference groups of weights [0, 0, 0, +1, 0, −1, 0, 0, 0], also of length $M$ each. These reference data are used for calibration and synchronization. The phase shift $\varphi$, though unknown, can be assumed constant along the symbol stream, as it varies slowly with respect to its total duration.

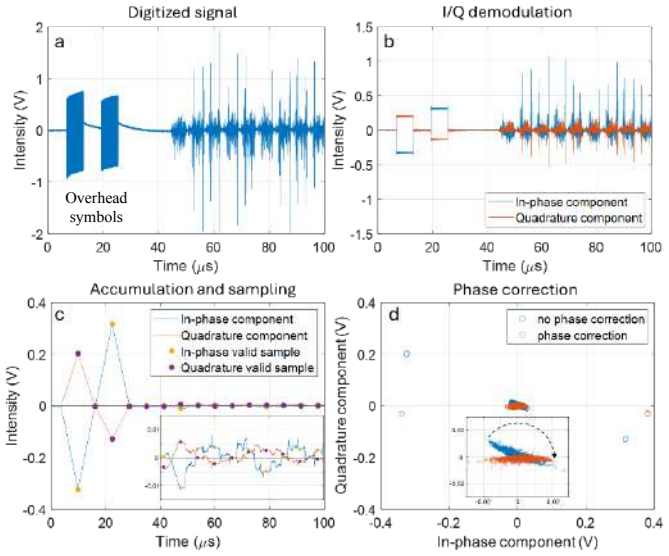


Fig. 3. Processing steps. (a) BPD signal. (b) Digital I/Q demodulation. (c) Accumulation and sampling at the I/Q channels. Inset: zoom of the accumulated and sampled output. The time scale is coincident with the main plot. (d) Complex I/Q plane of the accumulated and sampled output. The external points correspond to the +1 and –1 images. The inset shows the rotation corresponding to phase correction.

The detection consists of the steps showed in Fig. 3 for a MNIST trace, where $M$ = 784 and the symbol duration is $T$ = 8 ns, for a total duration of $MT$ = 6.272 µs. In a first stage we perform digital I/Q demodulation of the BPD signal with respect to the carrier frequency $f_s$. An example of a digitized BPD signal is shown in Fig. 3(a), where we observe the overhead data, followed by the first nine image × weight products. As the weights can be negative, the product symbols $s_k$ can be also negative, so that we need to recover the phase of the demodulated signal. The in-phase $I(t)$ and quadrature $Q(t)$ components of the BPD signal are:

$$I_{BPD}(t) = I_0 \cos(2\pi f_s t)\, I(t) - I_0 \sin(2\pi f_s t)\, Q(t) \qquad (2)$$

from which one can construct a complex signal

$$R(t) = I(t) + jQ(t) = e^{j\varphi} \sum_{k=-\infty}^{+\infty} s_k(t - kT) \qquad (3)$$

The in-phase and quadrature components are shown in Fig. 3(b), where we can notice the $\pi$ phase change between the two reference products followed by the demodulated data.

The final step is the detection of the scalar product of the weights and image, performing an accumulation process with a moving average over $M$ consecutive symbols and then sampling the output at intervals separated by $MT$. The output of this moving average filter and the sampled trace is shown in Fig. 3 (c). Here, the reference overheads, appearing as triangular signals, are used to synchronize the moving average with the sampling. The I/Q components of the sampled moving average provide a complex signal of the form $e^{j\varphi}\sum_{k=0}^{M-1} s_k$, from which the phase shift can be corrected, as shown in Fig. 3(d), and the actual value of the sought-for sum $\sum_{k=0}^{M-1} s_k$ be extracted.

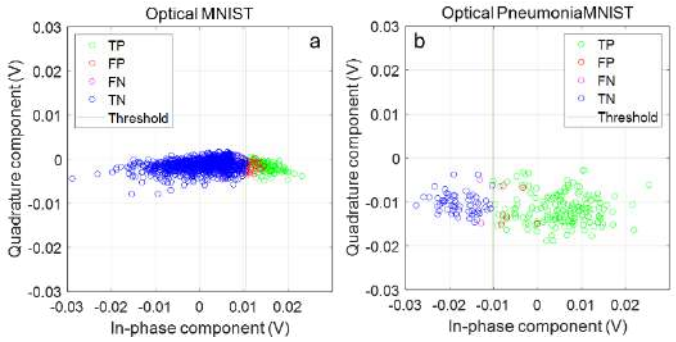


Fig. 4. Classification for the differencts databases used to validate the perfomance of the optical perceptron. (a) uses the MNIST database and is used to detect the the digit '6' among digits 0 through 9. (b) uses the PneumoniaMNIST database, where the objective is to detect the pneumonia in differents grayscale medical images.

With the phase shift corrected, we can perform detection on the real axis with positive and negative values. As in the computer perceptron, we define a threshold at which the test signals are correctly detected. This decision is made by evaluating the ROC curves and selecting a point that gives us a high true positive rate and a low false positive rate. This value is selected by maximizing the difference between the true positive and false positive rates at different thresholds. This process is performed on the computer and optical perceptrons using the same test data. The classification results for the different optical perceptron datasets are displayed in Fig. 4. Although the data consist of a cloud of points, the definition of a threshold enables the data to be separated into the two binary outputs of a perceptron. The figure also illustrates the various detection possibilities and the associated false positive and false negative error rates.

Table 1 shows the comparison between the performance of the optical and computer perceptrons for the different databases. In each of the database, the results are obtained from the same data for the optical and computer perceptron. Notice that the optical perceptron has a slight impact on accuracy compared to the computational perceptron; this difference is less than 2% for both databases. We also demonstrate that using a large, complex database does not affect the system's performance.

| Type of perceptron | Database | Size of images | Size of test | TP | FP | FN | TN | Accuracy (%) |
|---|---|---|---|---|---|---|---|---|
| Computer | MNIST | 28×28 | 1000 | 102 | 20 | 4 | 874 | 97,6 |
| Photonic assisted | Pneumonia MNIST | 28×28 | 1000 | 94 | 31 | 12 | 863 | 95,7 |
| Computer | MNIST | 64×64 | 460 | 328 | 8 | 14 | 110 | 95,2 |
| Photonic assisted | Pneumonia MNIST | 64×64 | 460 | 318 | 6 | 24 | 112 | 93,5 |

Table.1 Comparison of the classification results obtained by the computer, and by the photonic-assisted perceptron (TP: true positive, FP: false positive, FN: false negative, and TN: true negative).

## IV. Conclusion and Discussion

We have demonstrated a new photonic implementation of a perceptron. Our approach is based on a simple heterodyne interferometer setup. We have demonstrated a classification efficiency comparable to that of a computer-based perceptron. Our architecture offers a number of advantages. First of all, it can be easily implemented with integrated optics. Second, its intrinsic coherence opens up the prospect of new functionalities, such as the processing of complex data sets [7], the development of classification techniques in the complex plane, rather than just along the real axis, and the use of coherent I/Q detection instead of the digital processing used so far. Additionally, the proposed approach can be easily generalized to a multi-heterodyne architecture, for example using a frequency-shifting loop. This architecture, which has already proved its potential for analog computation in the real-time, enables multiplexing in the frequency domain [8]. The use of these architectures could provide gains of several orders of magnitude in terms of computing speed, compared with the single perceptron presented here, while leading to efficient implementation of photonic accelerators for convolutional neural networks [9-11].

## Acknowledgment

M.C.P. and C.R.F.P. acknowledge the support of the Agencia Estatal de Investigación (PID2020-120404GB-I00, EQC2019-006189-P). M.C.P. also acknowledges support from Ministerio de Universidades, Spain, Grant FPU21/05449. H.G.C. acknowledges support from Rennes Métropole (grant "Allocation d'Installation Scientifique" 2024). This research was also partly funded by Région Bretagne, FEDER, and Rennes Métropole (CPER PhotBreizh).

## References

[1] B. J. Shastri, A. N. Tait, T. Ferreira de Lima, *et al.* "Photonics for artificial intelligence and neuromorphic computing," Nat. Photonics, vol. 15, pp. 102–114, 2021.

[2] X. Xu, M. Tan, B. Corcoran, J. Wu *et al.*, "Photonic perceptron based on a Kerr microcomb for high-speed, scalable, optical neural networks," Laser Photonics Rev., vol. 14, no. 10, paper 2000070, 2020.

[3] T. Wang, S. Y. Ma, L. G. Wright, T. Onodera *et al.*, "An optical neural network using less than 1 photon per multiplication," Nat. Commun., vol. 13, paper 123, 2022.

[4] M. Mancinelli, D. Bazzanella, P. Bettotti, *et al.*, "A photonic complex perceptron for ultrafast data processing," Sci. Rep. vol. 12, paper 4216, 2022.

[5] L. Deng,"The MNIST database of handwritten digit images for machine learning research", IEEE Signal Process. Mag., vol. 29, no. 6 pp.141–142, 2012.

[6] J. Yang, R. Shi, D. Wei *et al.* "MedMNIST v2 – A large-scale lightweight benchmark for 2D and 3D biomedical image classification." Sci. Data, v ol. 10, no. 1, paper 41, 2023.

[7] Y. Xie, X. Ke, S. Hong, Y. Sun *et al.* "Complex-valued matrix-vector multiplication using a scalable coherent photonic processor," Sci. Adv., vol. 11, paper eads7475, 2025.

[8] G. Bourdarot, J.-P. Berger, and H. Guillet de Chatellus, "Multi-delay photonic correlator for wideband RF signal processing, " Optica, vol. 9, no. 4, pp. 325-334, 2022.

[9] H. Zhou, J. Dong, J. Cheng, W. Dong *et al.*, "Photonic matrix multiplication lights up photonic accelerator and beyond," Light Sci. Appl., vol. 11, paper 30, 2022.

[10] M. Chegini, Y. Guan, and J. Yao, "A microwave photonic processor for convolutional neural networks with increased effective speed of convolution," J. Lightw. Technol., in press, 2025.

[11] S. R. Kari, N. A. Nobile, D. Pantin, V Shah, and N. Youngblood, "Realization of an integrated coherent photonic platform for scalable matrix operations," Optica, vol. 11, no. 4, pp. 542-551, 2024.